https://doi.org/10.1016/j.jcsr.2016.08.011

Local web buckling of double-coped steel beam connections

Cheng Fang[a]*, Michael C. H. Yam[b], Angus C. C. Lam[c], Yunhao Liu[c] and K.F. Chung[d]

[a)] *Department of Structural Engineering, School of Civil Engineering, Tongji University, Shanghai 200092, China*

[b)] *Department of Building & Real Estate, The Hong Kong Polytechnic University, Hung Hom, Kowloon, Hong Kong SAR, China*

[c)] *Department of Civil & Environmental Engineering, University of Macau, Macau SAR, China*

[d)] *Department of Civil & Environmental Engineering, The Hong Kong Polytechnic University, Hung Hom, Kowloon, Hong Kong SAR, China*

**Corresponding author: email: chengfang@tongji.edu.cn, Tel: +86 21 65983894*

Abstract: This paper presents a comprehensive study on local web buckling behaviour of double-coped steel beam connections, cases which are common when beams of similar heights are joined. The study commenced with a series of full-scale tests on 11 specimens, covering a spectrum of cope lengths and cope depths. Local web buckling was observed as the main failure mode for most specimens. The ultimate load was found to decrease with increasing coped length and cope depth, and in addition, an increase of the rotational stiffness of the beam end connection could benefit the local web buckling capacity. A numerical study was subsequently performed enabling further interpretation of the test results. Good agreements were observed between the test results and finite element analysis predictions, and the stress conditions within the coped web panel at different loading stages were fully revealed. The numerical study also showed that the ultimate loads of some models were not sensitive to initial imperfection amplitudes, especially when the cope length was large (i.e. 450 mm or longer). It was believed that the imperfection insensitivity characteristic was due to the presence of post-buckling mechanism. Summarising the available test data, including the current test results and those previously reported by other researchers, design comments were made through comparisons against the existing design method. Conservative test-to-predicted ratios were generally shown, but unsafe predictions were obtained for some cases. A modification to the existing design approach was finally proposed for safer design of such connections.

Keywords: Double-coped beam; connections; local web buckling; full-scale tests; numerical study.

1. Introduction

In practical design of steel structures, the grillage beams often need to be coped at the beam end to avoid interference of the connected structural members thus to ensure the same elevation of the flanges of the beam at member intersections. Depending on specific design requirements, either the top or both top and bottom flanges of the beam end need to be removed, as shown in Fig. 1, and in either case, the load carrying capacity of the beam is inevitably compromised [1]. Coped beams can have different failure modes from those observed in their uncoped counterparts, and local web buckling is one of the most common failure modes at the coped region. Significant stress concentration can also be induced near the cope corner, which may further decrease the load carrying capacity [2]. Another common local failure mode for coped beams is 'block shear' which is featured by a fully or partially tearing-out of a block of material near the connection zone. In addition, lateral torsional buckling, a global instability failure mode, can more easily occur for coped steel beams compared with uncoped ones if insufficient lateral constraint is provided.

The structural response of coped beams has been studied by various researchers through either full-scale tests or numerical investigations. Cheng and Yura [3] reported ten tests on local web buckling response of top flange coped beams. Based on a subsequent numerical study, a plate buckling calculation model was developed for elastic local web buckling design of top (single) flange coped beams, and it was claimed that the proposed design provisions could give conservative results. The above design equations have been adopted by the AISC Steel Construction Manual [4]. Through conducting more local web buckling tests and numerical studies, Yam *et al.* [5] improved the plate buckling formula proposed by Cheng and Yura [3] to additionally consider the shear buckling phenomenon at the coped region. The modified calculation method was shown to agree better with the test results. Aalberg and Larsen [6] conducted six tests to study the local buckling response of top flange coped beams, where a simply-supported condition of the coped beam end (which was seated in a small steel block supported by a cylindrical bearing) was considered. Aalberg [7] later revisited those testing details and presented additional FE analysis. Based on the parametric study, a new design model incorporating a reduction factor for coped beam capacity was

finally developed to account for the effects of cope. Recently, more test data on the local web buckling behaviour of aluminium coped beams were provided by Aalberg [8], and it was found that the design model proposed by Yam et al. [5] could lead to better predictions than that proposed by Cheng and Yura [3]. Some researchers also proposed reinforcing strategies aiming to improve the local web buckling performance of coped beams through employment of various stiffener types, and those methods were found to be effective [9-10]. Apart from the studies on local web buckling, extensive investigations have also been conducted on the block shear [11-15] and lateral-torsional bucking [16-19] responses of coped beams. A comprehensive state-of-the-art review on local failures of coped beams was recently reported by Yam et al. [20].

However, it is noted that the emphasis of the previous research was mainly given to the response of top (compressive) flange single-coped beams, whereas there is limited information on the performance of double-coped beams. Double-coped beams are popular for the condition when beams of similar heights are joined, as illustrated in Fig. 1. Compared with the case of single-coped beams, more significant reduction of strength and stiffness may be induced in double-coped beams due to the removal of both beam flanges, and therefore, their behaviour needs to receive more attention. Cheng *et al.* [2] have undertaken a series of numerical studies on double-coped beams and proposed relevant design recommendations (hereafter named as the 'design method'). For practical design, it was suggested that the load carrying capacity (i.e. reaction) of double-coped beam connections could be sufficiently predicted by checking: 1) elastic local buckling capacity, 2) flexural yielding capacity, and 3) shear yielding capacity of the coped region, where the lowest value governs. Although the design recommendations were found to agree well with the numerical results, no physical test was conducted to further validate the design model until recently. Aalberg [8] conducted two tests on double-coped beams made of aluminum, one with welded end-plate and one with bolted double angle cleat connections. It was found that the connection type could have evident influence on the local web buckling capacity. Considering the design method [2], the test-to-predicted ratio for the coped beams with the two connection types were 0.83 and 1.36,

respectively (flexural yielding of the coped web governed). The authors [21] also performed five preliminary local web buckling tests on double-coped beams, where relatively large cope lengths ($c \geq 300$ mm) were employed to facilitate the observation of local web buckling mode. It was found that the design method tended to be conservative. These test data will also be included in the discussion of the current paper.

The main objective of this study is to help fill the knowledge gap in the area of local web buckling behaviour and design of double-coped beam connections. A total of 11 full-scale tests were conducted, covering a spectrum of coping details (including varying cope lengths and cope depths). A numerical study was subsequently carried out to enable further discussions on the stress distribution, buckling mechanism, and imperfection sensitivity of the specimens. Preliminary design recommendations were finally made through comparing the available test data pool against the existing design method.

2. Experimental programme

2.1 Test specimens

Six S460 UB406×140×39 test beams were ordered, and a total of 11 full-scale tests on double-coped beam connections were conducted. The main test parameters included cope length (c), cope depth (d_c), and the effect of end-plate connection rotational stiffness. The nominal dimensions for the top and bottom copes were identical for each specimen. The typical geometric configurations and key symbols of the test specimens are illustrated in Fig. 2(a), and the key dimensions of the coped web are given in Table 1. The end-plate connection type (with 10mm end-plate thickness) was employed for all the specimens, and double fillet welds were employed to connect the end-plate and the beam end. The depth of the end-plate (d_{ep}) was the same as the remaining web depth (h_o). For easy reference, each specimen was assigned with a test code, where 'C' represents nominal cope length (in mm), and 'dc' represents nominal cope depth (in mm). For specimen C550dc50R, the last letter 'R' represents the case of increased rotational stiffness of the end-plate connection, which was achieved through decreasing the gauge distance g (from 175 mm

to 90 mm) of the bolt hole, as shown in Fig. 2(a). The radius of the rounded cope corner was 15 mm for all the specimens. Photos of typical test specimens are given in Fig. 2(b). In the following discussions, for ease of understanding, the section along the boundary line between the coped and uncoped web panels is named as the 'end-of-cope section', as illustrated in Fig. 1. The top and bottom cope corners are also clearly marked in the figure.

The test specimens can be divided into two groups: the first group included those with cope length c up to 150 mm, which realistically represents typical coping details in normal building structures that employ profiled I-sections; the second group incorporated cope lengths ranging from 450 mm to 550 mm, reflecting more extreme cases. It was expected that the specimens in the first group failed by inelastic local web buckling, while those in the second group were expected to fail by elastic local web buckling. The main purpose of covering both failure modes in the current test programme was to fully examine the design method proposed by Cheng et al. [2]. For each test beam, both ends were coped with different coping details and they were considered as separate test specimens. When the test on one end was completed, the test beam was turned around for another test at the opposite end. The dimension of a typical test beam is shown in Fig. 3. Tension coupon tests were carried out to obtain the material property of the test beams, and the tests were conducted in a universal testing machine according to the ASTM A370 standard [22]. The Young's modulus, yield strength, and ultimate strength of the coped webs of the test beams are listed in Table 2.

2.2 *Test setup*

The test arrangement is schematically shown in Fig. 3. The statically determinate condition of the test beam allows measurements of cope end reaction via simple force equilibrium. The coped end (test end) of the beam was supported by the end-plate connection and the other end was supported by a roller support allowing horizontal movement and in-plane rotation. The test beams were loaded by a hydraulic jack with a maximum capacity of 1000 kN. Vertical stiffeners of 10mm thickness were applied at the loading and roller support locations to avoid local bearing failure. The distance between the loading point and the end plate was 900mm, such that the influence of

localized load bearing on the stress distribution in the coped region was negligible. Two load cells, one placed under the hydraulic jack and the other one at the roller support, were employed to measure the applied load (P) and the far end reaction (R_f), respectively. In this way, the cope end reaction R can be easily calculated via simple force equilibrium (i.e. $R = P - R_f$). The accuracy of both load cells is ±0.1% full scale. Lateral bracings were employed to prevent lateral-torsional buckling of the test beam, and the bracing locations are detailed in Fig. 3. Wood blocks were used between the steel lateral bracing and the flange tips to allow sliding between the flanges and the bracings. Snug-tightened M24 Grade 8.8 bolts were used to connect the end plate and the column flange. To facilitate the observation of elastic local web buckling of the specimens in the second test group, additional bolt washers were placed between the end plate and the supporting column face to form an approximately 4 mm gap between the end plate and the column face, as shown in Fig. 2(b). In this case the rotational stiffness of the end-plate connection could be further reduced. No such washers were employed for the first test group specimens, such that more realistic coped connection details in normal building frames could be reflected.

2.3 Instrumentation and test procedure

Longitudinal strain gauges and linear variable differential transformers (LVDTs) were used to measure the deformation and displacement of the test beams, as shown in Fig. 2(c). For the strain gauge arrangement, three sets of strain gauge rosette were employed to monitor the strain conditions over the end-of-cope section, i.e. along the boundary line between the coped and uncoped region. The strain gauges were applied at one side of the web. Additional strain gauges were applied to measure the strain conditions over the depth of the uncoped beam section near the coped region. Two LVDTs were placed at the loading point as well as at the beam flange near the coped region to monitor their vertical displacements, and additional LVDTs were employed to measure the lateral displacement of the coped web region. The web in the coped region was whitewashed for detecting any buckling line during the test.

A similar test procedure was generally employed for all the specimens. The load was applied by a manual pump jack. The loading process was mainly divided by two stages, namely, load control and stroke control. In the early stage, load control was used, and a constant load increment (5kN or 10kN) was applied for each interval. When nonlinear response of the test specimen was initially featured, the second loading stage, stroke control, was used to more reliably capture the nonlinear load-deflection response. During this stage, the load was adjusted to ensure a constant displacement increment (2mm or 3mm) at each step, and the loading equipment was held at regular intervals to obtain the static reading. The loading process terminated when the maximum lateral deflection recorded by the LVDTs reached about 25mm, and the test beams were gradually unloaded afterwards. All data were recorded by an automatic data acquisition system.

3. Test results and discussions

3.1 General

The main test results, including the ultimate load P_u, the deflection at loading position at ultimate load δ, and ultimate reaction R_u (i.e. $R_u = P_u - R_{fu}$, where R_{fu} = far end reaction at ultimate load)), are given in Table 3. The ultimate reactions of the specimens ranged from 72.2 kN to 372.8kN, varying with different coping details. Considering the static equilibrium condition of the test beam, the ultimate end moment M_u at the coped end (i.e. $M_u = P_u \times 0.9\text{m} - R_{fu} \times 2.4\text{m}$) were also calculated, as given in Table 3. The coped end moments, which were induced by the rotational stiffness of the end-plate connection, ranged between 39.1 kNm and 59.6 kNm for the specimens with short copes, and the negative moment might influence the local web buckling behaviour of these specimens. For the specimens with long cope lengths, the moment induced at the coped end was insignificant due to the presence of the gap between the end-plate and column face.

3.2 Failure modes

Local web buckling was observed as the main failure mode for most specimens. Typical buckling shapes of the specimens are shown in Fig. 4, where buckling lines are clearly found. For the specimens with cope length up to 150 mm (i.e. the first group), the buckling line only became

evident at relatively late stages, i.e. after ultimate load. This implied that the ultimate load of those specimens with relatively small cope lengths was probably governed by inelastic local web buckling, i.e. local yielding occurred prior to buckling. The buckling line was extended from the top edge of the coped web towards the bottom edge with an orientation of approximately 45º angle from the vertical line. When the buckling line was fully developed, evident lateral deflection was observed over the top edge of the cope, whereas much less significant lateral deflection was observed along the bottom edge. At late post-ultimate stages, the top flange near the coped region started to move laterally (accompanied by rotation) due to the lack of lateral restraints provided immediately near the coped region, as shown in Fig. 4.

It should be noted that for specimens C80dc25, C80dc35, C80dc50, and C150dc25, yielding of the uncoped beam section at the loading position occurred at ultimate load. According to the coupon test results, it was calculated that specimens C80dc50 and C150dc25 only experienced partial cross-sectional yielding at the loading position when the ultimate load was achieved, but for specimens C80dc25 and C80dc35, full plastic hinge was developed over the beam cross-section at the loading point at ultimate load. The early yielding of the beam section also suggested that these specimens with small cope lengths had very good load carrying capacity against local web buckling. It is worth mentioning that for the specimens whose ultimate loads were governed by the formation of plastic hinge, a buckling line was also developed over the coped region at late loading stages. This was due to the considerable lateral movement of the top flange because of the lack of lateral restraints provided at the flanges immediately near the coped region.

For the specimens with larger cope length (i.e. the second group), the ultimate load was all governed by typical local web buckling at the cope, and no beam yielding was developed at the loading point. The buckling line was extended from the top edge of the coped web towards the bottom edge with an orientation of approximately 20º angle from the vertical line. In addition, the buckling line tended to initiate from approximately 1/4 to 1/3 length (from the end of the cope) of the top edge of the cope, a case which was different from the first group specimens where the

buckling line normally started from either the top cope corner or the end of the beam near the end-plate. For most cases, lateral deflections were observed for both the top and bottom edges of the coped web, although the lateral deflection along the top cope edge was larger than that along the bottom cope edge. This is obviously different from the typical deflection pattern of top flange single-coped beams where no lateral deflection was developed at the bottom flange due to the restraints provided by the uncoped bottom flange, as reported by relevant researchers [2-3]. The difference of the buckling pattern between the cases of single-coped and double-coped beams revealed the necessity of proposing appropriate design rules specifically for the latter case. By the end of the test, no lateral movement of the top flange near the coped region was induced for the second group specimens due to the presence of the lateral restraints that were close to the end-of-cope section.

3.3 Load-deflection response

The load versus vertical in-plane deflection curves for all the specimens are shown in Fig. 5(a). Linear behaviour was generally observed from the beginning of the load until approximately 80% - 95% of the ultimate load, and afterwards nonlinear response was developed. For some specimens, obvious nonlinear response was observed before reaching the corresponding ultimate load, which indicated that yielding of web at the coped region and of the section at the loading point could have been developed during this stage. After ultimate load, the sustained load started to decrease with moderate dropping rates, and the test was terminated when excessive deflection was developed. No sudden failure was induced beyond ultimate load.

The load versus coped web lateral deflection responses of typical specimens are shown in Fig. 5(b). It was found that lateral deformation started to be developed when the applied load exceeded approximately 10% of the ultimate load, and then the deformations increased gradually but were generally kept at low levels, i.e. less than 2 mm. It seemed that the lateral deformation pattern of the coped web did not follow any particular trend prior to 80% of the ultimate load, and this could be due to irregular initial imperfection shapes of the coped web region. When the applied

load reached around 90% of the ultimate load, the lateral deformation started to be evident at some locations, a sign of the inception of local web buckling. The measured lateral displacements were in line with the visual test observations. For the specimens with short copes, e.g. specimens C80dc25 and C150dc25, the maximum lateral displacement was recorded by LVDT4 (locations are given in the figure), which was close to the 'buckling line' passing through the top cope corner. For the specimens with long copes, e.g. specimens C450dc25 and C550dc25, the maximum lateral displacement was captured by LVDT3, which coincided with the buckling line initiating from approximately 1/4 to 1/3 cope length from the end-of-cope section. In addition, it was observed that the lateral deflections for the specimens with smaller cope lengths were less than those with larger cope lengths.

3.4 Strain distributions

Typical normal stress distributions over the end-of-cope section for selected specimens are shown in Fig. 6(a). As the strain gauge readings might be unreliable at the inelastic stage, the load levels considered in the figure were less than 80% of the ultimate load, i.e. the strain gauge readings were expected to be mainly in the elastic range. The calculated ('theoretical') strain distributions were also included for comparison purposes, and it should be noted that the calculated values were derived taking account of the negative moment induced at the coped end. Therefore, the bending moment at the considered section (end-of-cope) was calculated based on the bending moment diagram as illustrated in Fig. 6(b). It was observed that with increasing applied load, the trend of the test strain distributions agreed reasonably well with the theoretical calculations. The test neutral axis was generally in line with the theoretical one which is along the mid depth of the double-coped web. It was also confirmed that all the strain gauge readings were within the elastic range for the considered load levels, which echoed the aforementioned load-deflection responses where the specimens generally behaved elastically prior to 80% of the ultimate load.

For most specimens, the test strains seemed to show better agreements with the calculated values at earlier loading stages, e.g. 20% of the ultimate load, whereas with increasing load, more

evident discrepancy was observed, especially at the compressive strain region. It was believed that the discrepancy was due to the initial imperfection which led to minor out-of-plane plate bending action over the coped web at the compressive region. This has been confirmed via the load vs. lateral deflection responses as previously discussed in Section 3.3. As the strain gauges were only applied at one side of the web, their readings were affected by the plate bending action which caused non-uniform stress/strain over the web plate thickness. This may also explain the less evident discrepancy over the tension region of the coped web where the effect of out-of-plane plate bending was not remarkable due to the stretching action over the tension coped region. Finally, it is worth mentioning that as there was no strain gauge directly mounted near the cope corners, the possible stress concentration effect could not be well reflected by the current strain gauge readings. In order to better understand the strain/stress distribution in the web within the coped region, numerical investigation of the specimens was conducted and will be discussed in Section 4.

3.5 Factors influencing the ultimate reaction

The cope length-to-beam depth (c/D) and cope depth-to-beam depth (d_c/D) ratios are normally considered as two representative variations that could affect the local web buckling behaviour of coped beams [2-3]. In this study, the considered c/D ratio ranged between 0.201 to 1.382, and the corresponding ultimate reactions R_u with varying c/D ratios are shown in Fig. 7. It was observed that R_u significantly decreased with increasing c/D ratios. When the c/D ratio increased from 0.201 to 1.382, the value of R_u could be reduced by approximately 80%. It was obvious that the decrease of R_u with increasing c/D ratio was due to the increase of the 'buckling length', i.e. the length of the coped web. In addition, the hogging bending moment induced by the end-plate connection could have more remarkable influence on the specimens with short copes (lower c/D ratios), where the entire cope length could be simultaneously subjected to both hogging and sagging bending moments. In this case, local web buckling was less easily to occur for these specimens, recalling that for specimens C80dc25 and C80dc35, plastic hinge was first formed over

the beam section at the loading point and the applied load which would cause inelastic local web buckling might be higher than that caused plastic bending failure of the uncoped section.

It is also worth mentioning that for the cases of c/D ranging from 1.131 to 1.382, the rotational stiffness of the end-plate connection was deliberately decreased with additional washers applied between the end-plate and column face. The ultimate reaction of those specimen could be increased if the same end-plate connection condition was employed (i.e. no washers), such as the case of the specimens with lower c/D ratios. The influence of rotational stiffness of the end-plate connection can be confirmed through comparing specimen C550dc50 with C550dc50R, where a decreased gauge distance (g) of the end-plate was employed for the latter case in order to increase the connection rotational stiffness. It was found that the ultimate reaction was increased by 10.7% when g decreased from 175 mm to 90 mm. Again, the increase of R_u could be due to more significant hogging bending moment induced at the coped end, which tended to decrease the 'effective' buckling length of the coped web. As only one comparison group was considered in the current study to examine the effect of connection rotational stiffness, more experimental and numerical investigations may be required on this front.

For the influence of the cope depth (d_c), the considered d_c/D ratio ranged between 0.063 and 0.126, and the corresponding ultimate reaction R_u with varying d_c/D ratios are shown in Fig. 7. It was shown that the d_c/D ratio could also have evident influence on R_u which was on average decreased by 17.7% when the d_c/D ratio increased. The decrease of R_u was mainly caused by an increased level of compressive stress along the top edge of the coped web due to decreased elastic section modulus.

4. Numerical study and further discussions

4.1 General

Since the stress concentration effect, which may play a key role in affecting the local web buckling behaviour of double-coped beams, was not fully revealed in the current test programme, a numerical study could enable further interpretation of the test results. For the specimens

experiencing the formation of plastic hinge at the loading point, the actual local web buckling resistance could be obtained through numerical predictions. Furthermore, as the detailed imperfection pattern of the coped web was not measured before the tests, the numerical study could shed light on the influence of initial imperfections on the local web buckling performance of the specimens.

4.2 Modelling strategy

The nonlinear finite element (FE) analysis package ABAQUS [23] was employed for the numerical study. Four-node quadrilateral shell elements (S4R) with reduced integration were used to discretize the members. The boundary conditions were appropriately defined to reflect the actual testing condition. It should be noted that a very minor vertical displacement of the end-plate was observed at the coped end during the tests of some of the specimens, and this was probably due to the slippage between the end-plate and column face (e.g. due to bolt hole clearance) and was also possibly due to slight settlement of the supporting frame [24]. This effect was also considered in the FE model, where linear vertical spring elements were applied to support the end-plate.

An isotropic elastic–plastic material model with the von Mises yield criterion was employed, where the stress-strain response was obtained from the coupon tests and was then converted to true stress/strain used for the FE model. Two steps, namely, eigenvalue analysis and nonlinear Riks analysis, were adopted to obtain the nonlinear buckling behaviour of the coped beams. The first step, eigenvalue analysis, was mainly used to obtain the lowest elastic buckling mode. This buckling mode is normally considered as the initial geometric imperfection shape which was then incorporated for the second step where a nonlinear Riks analysis was conducted to trace the nonlinear buckling response of the coped beams. Different amplitudes of imperfection can be taken in the second step. The typical fundamental buckling modes for the specimens are shown in Fig. 8(a).

4.3 Results of FE modelling and discussions

Six representative test specimens, C80dc25, C80dc50, C150dc25, C150dc50, C550dc25, and C550dc50, were selected. The selected specimens cover a reasonable range of test parameters (i.e. c and d_c), such that the influence of the varying parameters could be sufficiently revealed. Fig. 9 shows the comparisons of the load-deflection (P-δ) responses obtained from the tests and FE study, where three initial imperfection amplitudes, namely, 0.1 mm, 0.5 mm, and 2.0 mm, were considered. Good agreements can be seen between the test results and FE predictions, especially in terms of the initial loading response and ultimate load.

An interesting and important finding is that the models with long copes (e.g. c = 550 mm) show little sensitivity to initial imperfection amplitudes in terms of ultimate load, whereas for the models with 80 mm and 150 mm cope lengths, moderate sensitivity is shown. In order to investigate this phenomenon, the elastic buckling load of the fundamental-mode for each model was obtained from the eigenvalue analysis and is included in the load-deflection response, i.e. Fig. 9. It can be seen that the ultimate load of the specimen with 80 mm or 150 mm cope length is less than the elastic buckling load, and this is due to the fact that those models fail in an inelastic local web buckling manner. For models C550dc25 and C550dc50, however, the ultimate load exceeds the elastic buckling load, which suggests that a post-buckling resisting mechanism is developed after initial local buckling, and therefore the ultimate load is not sensitive to imperfection. To further confirm this, Fig. 10 additionally shows the load vs. lateral deflection responses (at maximum lateral movement locations) of specimens C150dc50 and C550dc50. It is clearly observed that for specimen C150dc50, the lateral deformation of the cope corner only starts to be obvious when the applied load gets close to the ultimate load. In other words, the inception of inelastic local web buckling is accompanied by a ‘relatively sudden’ increase of the cope corner lateral deformation, and it is sensible to deduce that an increased imperfection amplitude can cause earlier development of such lateral deformation, and thus earlier inelastic local web buckling. For specimen C550dc50, on the other hand, the maximum lateral deformation of the coped region (i.e. the top edge of the cope) starts to be developed at an early stage. After the development of the lateral deformation, the

resistance keeps increasing. When the ultimate load is achieved, the maximum lateral deformation has already been significantly developed (approximately 25 mm). This lateral deflection response echoes the previous findings that the ultimate load is insensitive to the imperfection due to the presence of post-buckling mechanism.

Fig. 10 also reveals the stress development conditions at different loading stages, where the stresses at the mid-thickness of the shell elements (i.e. values read from the mid-thickness integration point) are selected and shown. For specimen C150dc50, stress concentration is induced near both cope corners (top and bottom ones) at early loading stages. When the applied load reaches 427kN (84% of the ultimate load), significant yielding has been developed at the cope corners, but no obvious lateral deformation is induced at this stage. This confirms that the failure mode of the model is governed by inelastic local web buckling, noting that the buckling line of this specimen is initiated near the very top cope corner. At ultimate load (507.9 kN), the area of yielding further spreads towards the main part of the coped web, but no evident buckling line has been formed at this moment. With further increase of deflection, the resisting load starts to drop, which is accompanied by significant lateral deformation of the coped region. Concurrently, the buckling line is propagated from the top cope corner to the uncoped region of the web with an orientation of approximately 45º angle from the vertical line, and this pattern agrees very well with the test observation. The centre part of the coped web is also significantly yielded after reaching the ultimate load.

For model C550dc50, the stress contour also shows stress concentration effect at the initial loading stage, but this effect only becomes evident when the applied load approaches the ultimate load, e.g. 90.6 kN (88% of the ultimate load). Under this level of load, the maximum lateral deformation of the coped web has become significant, which indicates that local web buckling has been induced. It is also found that at 90.6 kN, only the cope corners experiences minor yielding due to stress concentration, while no yielding is developed at any other part of the web. In particular, no yielding is developed near 1/3 length (from the end of the cope) of the top cope edge at which the

first buckling line is developed. This indicates that the model mainly exhibits elastic local web buckling mode. When the ultimate load (102.6 kN) is achieved, a clear buckling line has been developed, initiating at 1/4-1/3 length (from the end of the cope) of the top edge of the cope and then propagates downwards with an orientation of around 20º angle from the vertical line; concurrently, evident yielding is developed at the bottom edge of the cope near the bottom cope corner. Again, the buckling line predicted by the FE model agrees very well with the test observations. Beyond the ultimate load, the resistance starts to decrease, and the major buckling line propagates over the entire depth of the coped web. At the same time, another buckling line (as marked in Fig. 10) is developed over the centre region of the coped web panel with an orientation of approximately 55º angle from the horizontal line. There could be an interaction of shear and bending behaviour in the coped region which could initiate the buckling behaviour

The FE model may also help predict the actual local web buckling resistance of the specimens that failed by the formation of plastic hinge. Taking specimen C80dc25 for example, the test ultimate load was 581.9 kN (leading to an ultimate reaction R_u of 372.8 kN), but the actual local web buckling resistance $R_{u\text{-}actual}$ may be much higher. In order to obtain $R_{u\text{-}actual}$, the uncoped beam section needs to be strengthened, and therefore, the flanges of model C80dc25 was deliberately increased to 15 mm, such that the plastic hinge would not be formed before the initiation of local web buckling. A moderate imperfection of 0.5 mm was selected for the modified model. The new FE results show that the failure mode of the model is now featured by inelastic local web buckling rather than the formation of plastic hinge, and the ultimate load is 862.2 kN with the corresponding $R_{u\text{-}actual}$ = 546.4 kN (46.6% higher than that given by the test result). The inelastic local web buckling mode of model C80dc25 is shown in Fig. 8(b).

Generally speaking, the FE study shows that the double-coped beams with relatively short copes exhibit inelastic local web buckling failure, whereas those with long copes tend to fail by elastic local web buckling. For the latter case, post-buckling resistance can be developed, which attributes to the findings that those models are insensitive to initial imperfection amplitudes.

Importantly, the main structural responses, including failure mode and ultimate load, are well predicted by the FE models.

5. Design comments

The local web buckling strength of double-coped beams was first investigated by Cheng et al. [2] via elastic FE studies, based on which a design approach was proposed which was later adopted by the AISC Steel Construction Manual [4]. The design approach assumed a simple lateral-torsional buckling model with an unbraced length of c and a linearly-increased bending moment diagram. The critical moment M_{cr} was determined by:

$$M_{cr} = f_d \left(\frac{\pi}{c}\right)\sqrt{EI_y GJ} \tag{1}$$

where f_d = an adjustment factor taken as f_d = 3.5 - 7.5(d_c/D) to conveniently account for various influential factors such as stress concentration and shear stress, E = Young's modulus, $I_y = h_o t_w^3/12$, G = shear modulus, and $J = h_o t_w^3/3$ (symbols have been defined in Fig. 2(a)). It was also suggested that for practical design, the load carrying capacity (i.e. reaction) of double-coped beam connections could be safely predicted by checking three items: 1) elastic local web buckling capacity R_{cheng}, 2) flexural yielding capacity R_y, and 3) shear yielding capacity R_{vy} of the coped region, where the lowest value governs. For elastic local web buckling, the ultimate reaction R_{cheng} can be obtained by $R_{cheng} = M_{cr}/(c+t_{ep}/2)$, where t_{ep} = thickness of the end-plate. Similarly, the ultimate reaction R_y can be obtained by $R_y = M_y/(c+t_{ep}/2)$, where M_y = elastic yield moment of the coped web.

With more available test data emerging recently, it is necessary to revisit the existing design recommendation which was purely based on an early numerical work conducted in the 1980s with no physical test evidence available at that time. Apart from the 11 specimens conducted in this study, the five preliminary local web buckling tests on double-coped beams previously conducted by the authors [21] as well as the two tests on aluminium double-coped beams recently conducted by Aalberg [8] were also included in the current discussion. It is worth mentioning that the test specimens for the previous tests [21] were conducted on S355 UB356×127×33 beams and the cope

corners were not rounded (i.e. sharp cope corner remained). The ultimate reactions of these specimens obtained from the three checking items, i.e. R_y, R_{vy}, and R_{cheng}, are given in Table 3, where the measured material properties were employed to calculate these values. The lowest value, which governs the design, is highlighted using bold fonts in the table.

It is shown that the design ultimate reactions for the considered specimens can be governed by all the three possible failure modes, i.e. flexural yielding (based on first yield), shear yielding, and elastic local web buckling, and as expected, flexural yielding and shear yielding tend to govern the failure mode of the specimens with short copes, whereas elastic local web buckling is main governing design failure mode for the case of long copes. Using the design method, the test-to-predicted ratios and the associated coefficients of variation (CoVs) are obtained, as given in Table 3. It should be noted that the results for specimens C80dc25 and C80dc35 were not considered for the calculations of average test-to-predicted ratio and CoV, as their test ultimate reactions were not governed by local web buckling. The comparison results generally show that the design method proposed by Cheng et al. [2] could lead to safe predictions, but the level of dispersion is large. The average test-to-predicted ratio is 1.424, and the associated CoV is 0.262. Importantly, unsafe predictions are provided from the design method for the specimens with relatively short cope length (e.g. c = 150 mm or less). On the other hand, the conservative predictions for the cases of long cope can be due to the conservative curve fitting approach, as detailed in Cheng et al. [2]. In addition, a perfect simply-supported condition was assumed in Cheng's numerical studies, whereas in actual cases as well as in the current test conditions, a certain level of beam end connection stiffness exists, which tend to increase the ultimate reaction.

From practical design point of view, the elastic local web buckling design approach proposed by Cheng et al. [2] may still be viable as it can provide safe predictions and thus be able to cover different conditions of beam end connections, i.e. provide a lower bound for the elastic local web buckling design resistance. For the calculation of R_y, however, a reduction factor may be required to ensure safe design. Based on the limited test data, a factor of 0.7 is provisionally

recommended for R_y. Adopting this value, the new test-to-predicted ratios for specimens C80dc50, C150dc25, and C150dc50 are 0.97, 1.26, and 1.38, respectively, which makes the design much safer. It should be mentioned that this reduction factor is only applicable to the case of short copes. According to the available test results, it is preliminarily suggested that the factor is used when $c \leq$ 150 mm.

In light of the above, the following preliminary design strategies are recommended for double-coped beam connections based on the limited test data: 1) for the case of $c \leq 150$ mm, a reduction factor is applied to R_y, where a provisional value of 0.7 is proposed; 2) the original calculation method for R_{vy} still holds; and 3) the original calculation method for R_{cheng} still holds. Again, the lowest value governs the design resistance. Employing this procedure, safe design could generally be achieved for a wide range of coping details. It should be noted that the modified design approach does not consider the effects of connection rotational stiffness, connection type (e.g. double cleat angles or end-plate connections), and lateral restraints along the beam length, nor any reliability analysis has been carried out. Therefore, more extensive experimental and numerical studies may be required in order to stipulate more sophisticated and reliable local web buckling design rules for double-coped beam connections.

6. Summary and conclusions

This paper reported an experimental and numerical study on local web buckling behaviour and design of double-coped steel beam connections. A total of 11 full-scale tests were conducted, and the main test parameter included cope length, cope depth, and beam end connection stiffness. Local web buckling, featured by clear buckling line being developed over the coped web, was observed as the main failure mode for most specimens. However, for some specimens with the shortest cope (c = 80 mm), yielding of the beam occurred first at the loading position due to relatively high local web buckling resistance. The cope length-to-beam depth (c/D) and cope depth-to-beam depth (d_c/D) ratios were found to be the two important variations that evidently affected the ultimate resistance R_u of the specimens. When the c/D ratio was increased from 0.201 to 1.382, R_u

could be reduced by approximately 80%. When the d_c/D ratio was increased from 0.063 to 0.126, R_u was on average decreased by 17.7%. The beneficial influence of increased rotational stiffness of the end-plate connection was also exhibited, where it was found that R_u could be increased by 10.7% when the bolt gauge of the end-plate was decreased from 175 mm to 90 mm. It is worth mentioning that these test results are based on the currently considered lateral restraining conditions. Changing the boundary conditions may lead to varying local web buckling resistance.

The subsequent numerical study showed good agreements between the FE predictions and test observation, especially in terms of failure mode and ultimate load. It was clearly shown that the double-coped beam specimens with relatively short copes exhibit inelastic local web buckling failure, whereas those with long copes tend to fail by elastic local web buckling. For the latter case, the models were found to be insensitive to initial imperfection amplitudes, which was attributed to the development of post-buckling resistance. The FE study also comprehensively revealed the stress development conditions within the coped web panel, where the stress concentration effect was clearly seen near the top and bottom cope corners. The FE models also showed that if yielding was avoided over the beam cross-section at the loading point, the resulting ultimate load governed by local web buckling could be evidently higher than that given by the test result.

Through collecting the available test data including the current test results and those reported by other researchers, design comments were made by comparing the test results against the existing design method. The average test-to-predicted ratio was 1.424, indicating generally a safe design, and the associated CoV was 0.262. However, it was found that the design method could lead to unsafe predictions for the specimens with relatively short copes, e.g. c = 150 mm or less. It was believed that the unsafe results were probably due to the exclusion of the stress concentration effect near the cope corners when calculating the flexural yielding capacity. To ensure a safe design catering for a sufficiently wide range of coping details, a slightly modified design approach was proposed, where the change was to apply a reduction factor for the ultimate reaction R_y governed by flexural yielding of the coped region. The basic design concept, i.e. taking the lowest value of R_y,

R_{vy}, and R_{cheng}, still holds, and as a result a lower bound local web buckling capacity for double-coped beam connections could be generally obtained.

7. Acknowledgements

The work described in this paper is fully supported by a grant from the Research Grants Council of the Hong Kong Special Administrative Region, China (Project No. PolyU 5288/13E). The assistance of Mr. Ka Man Tou in conducting the tests is also gratefully acknowledged.

References

[1] Milek WA. A cautionary note on beam copes. Engineering Journal 1980; 17(3):72-3.

[2] Cheng JJ, Yura JA, Johnson CP. Design and behavior of coped beams. Ferguson Structural Engineering Laboratory Report No. 84-1, Department of Civil Engineering, University of Texas; July 1984.

[3] Cheng JJR, Yura JA. Local web buckling of coped beams. Journal of Structural Engineering, ASCE 1986;112(10):2314-31.

[4] American Institute of Steel Construction. Steel Construction Manual 14th Edition. One East Wacker Drive, Suite 700, Chicago, Illinois, 2011.

[5] Yam MCH, Lam ACC, Iu VP, Cheng JJR. The local web buckling strength of coped steel I-beam. Journal of Structural Engineering, ASCE 2003;129(1): 3-11.

[6] Aalberg A, Larsen PK. Local web buckling of coped beams. In: Proceedings of Nordic Steel Construction Conference NSCC 2001, Helsinki, Finland, 2001.

[7] Aalberg A. Experimental and numerical parametric study on the capacity of coped beam ends. Journal of Constructional Steel Research 2015;113:146-55.

[8] Aalberg A. Design of aluminium beam ends with flange copes. Thin-Walled Structures 2015;94:593-602.

[9] Yam MCH, Lam ACC, Wei F, Chung KF. The local web buckling strength of stiffened coped steel I-beam. International Journal of Steel Structures 2007;7(2):129–38.

[10] Yam MCH, Ma HW, Lam ACC, Chung KF. Experimental study of the strength and behaviour of reinforced coped beams. Journal of Constructional Steel Research 2011;67: 1749–1759.

[11] Franchuk CR, Driver RG, Grondin GY. Experimental investigation of block shear failure in coped steel beams. Canadian Journal of Civil Engineering 2003;30(5):871-81.

[12] Driver RG, Grondin GY, Kulak GL. Unified block shear equation for achieving consistent reliability. Journal of Constructional Steel Research 2006;62:210-22.

[13] Topkaya C. Finite element modeling of block shear failure in coped steel beams. Journal of Constructional Steel Research 2007;63(4):544-53.

[14] Fang C, Lam ACC, Yam MCH, Seak KS. Block shear strength of coped beams with single-sided bolted connection. Journal of Constructional Steel Research 2013;86:153-66.

[15] Lam ACC, Fang C, Yam MCH, Wang W, Iu VP. Block shear strength and design of coped beams with double bolt-line connections. Engineering Structures 2015;100: 293-307

[16] Cheng JJR, Yura JA, Johnson CP. Lateral buckling of coped steel beams. Journal of Structural Engineering, ASCE 1988;114(1):1-15.

[17] Lam CC, Yam MCH, Iu VP, Cheng JJR. Design for lateral torsional buckling of coped I-beams. Journal of Constructional Steel Research 2000;54:423-43.

[18] Maljaars J, Stark JWB, Steenbergen HMGM, Abspoel R. Lateral–torsional buckling resistance of coped beams. Journal of Constructional Steel Research 2005; 61(11):1559-75.

[19] Gupta AK. Buckling of coped steel beams. Journal of Structural Engineering, ASCE 1984;110(9):1977-87.

[20] Yam MCH, Fang C, Lam ACC, Cheng JJR. Local failures of coped steel beams – a state-of-the-art review. Journal of Constructional Steel Research 2014;102:217-32.

[21] Fang C, Yam MCH. Local web buckling strength of double coped steel beams. In: Proceedings of the Second Australasia and South-East Asia Structural Engineering and Construction Conference Bangkok, Thailand, November 3–7, 2014.

[22] ASTM A370, Standard test methods and definitions for mechanical testing of steel products. American Society for Testing and Material, Philadelphia, PA, 2002.

[23] ABAQUS Analysis User's Manual. ABAQUS Standard, Version 6.12; 2012.

[24] Yam MCH, Chung KF. A numerical study of the strength and behaviour of reinforced coped beams. Journal of Constructional Steel Research 2013;80:224-34.

List of figures

Fig. 1 Practical coping details of steel beams

Fig. 2 Test specimens: a) specimen details and key symbols, b) photos of typical specimens, c) instrumentations

Fig. 3 Schematic illustrations and photos of test setup

Fig. 4 Typical failure modes of specimens

Fig. 5 Test results: a) load-vertical deflection response, b) load-horizontal deflection response

Fig. 6 Strain conditions: a) typical strain distributions, b) calculation method of strain

Fig. 7 Influences of coping details on ultimate reaction

Fig. 8 Finite element analysis results: a) fundamental mode by eigenvalue analysis, b) local web buckling failure of ‘modified’ model C80dc25

Fig. 9 Comparisons of load-deflection responses between test results and FE predictions

Fig. 10 Detailed load-deflection responses and stress conditions of typical specimens

List of tables

Table 1 Key dimensions of specimens – measured values

Table 2 Coupon test results for beam webs

Table 3 Summary of test results and design predictions

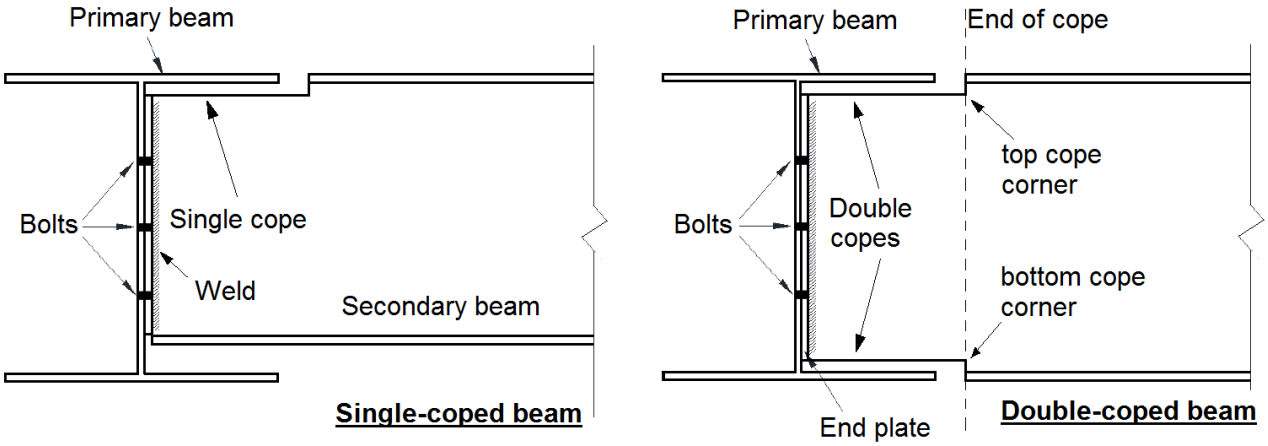

Fig. 1 Practical coping details of steel beams

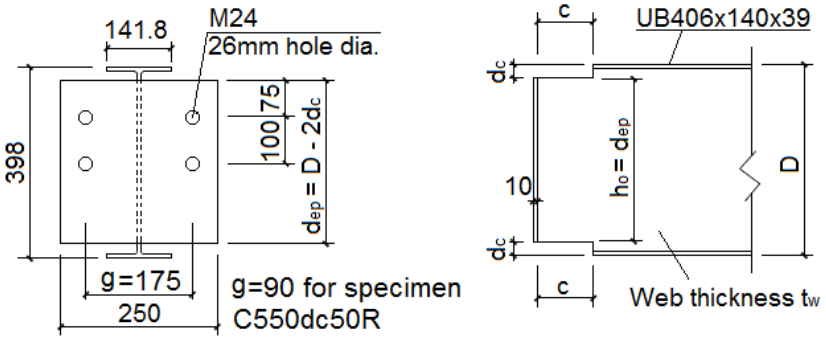

(a)

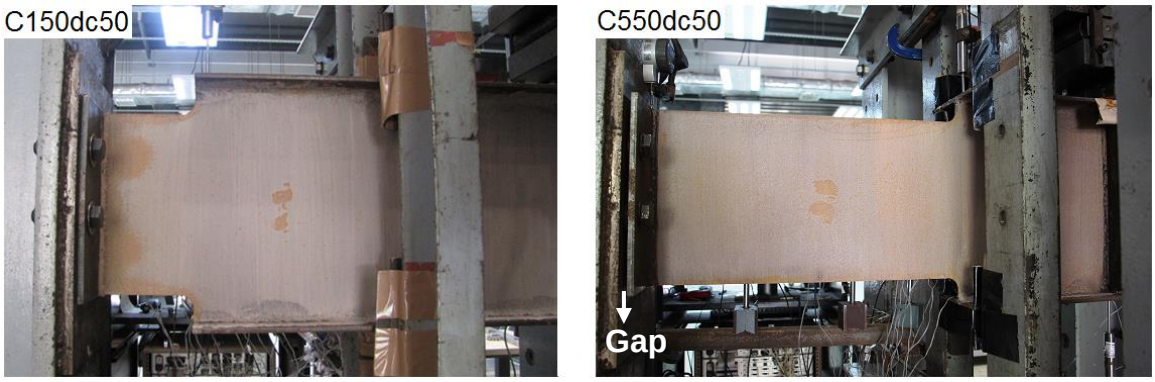

(b)

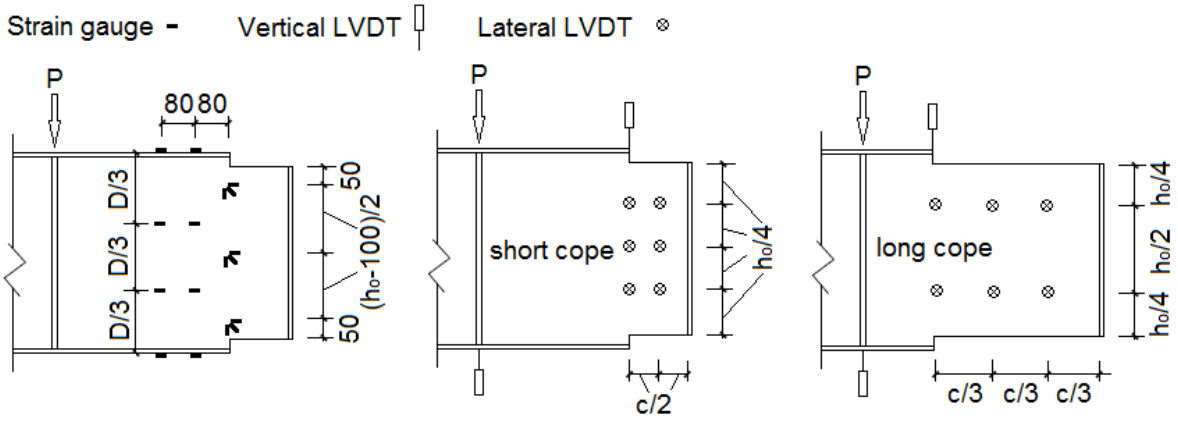

(c)

Fig. 2 Test specimens: a) specimen details and key symbols, b) photos of typical specimens, c) instrumentations (not-to-scale)

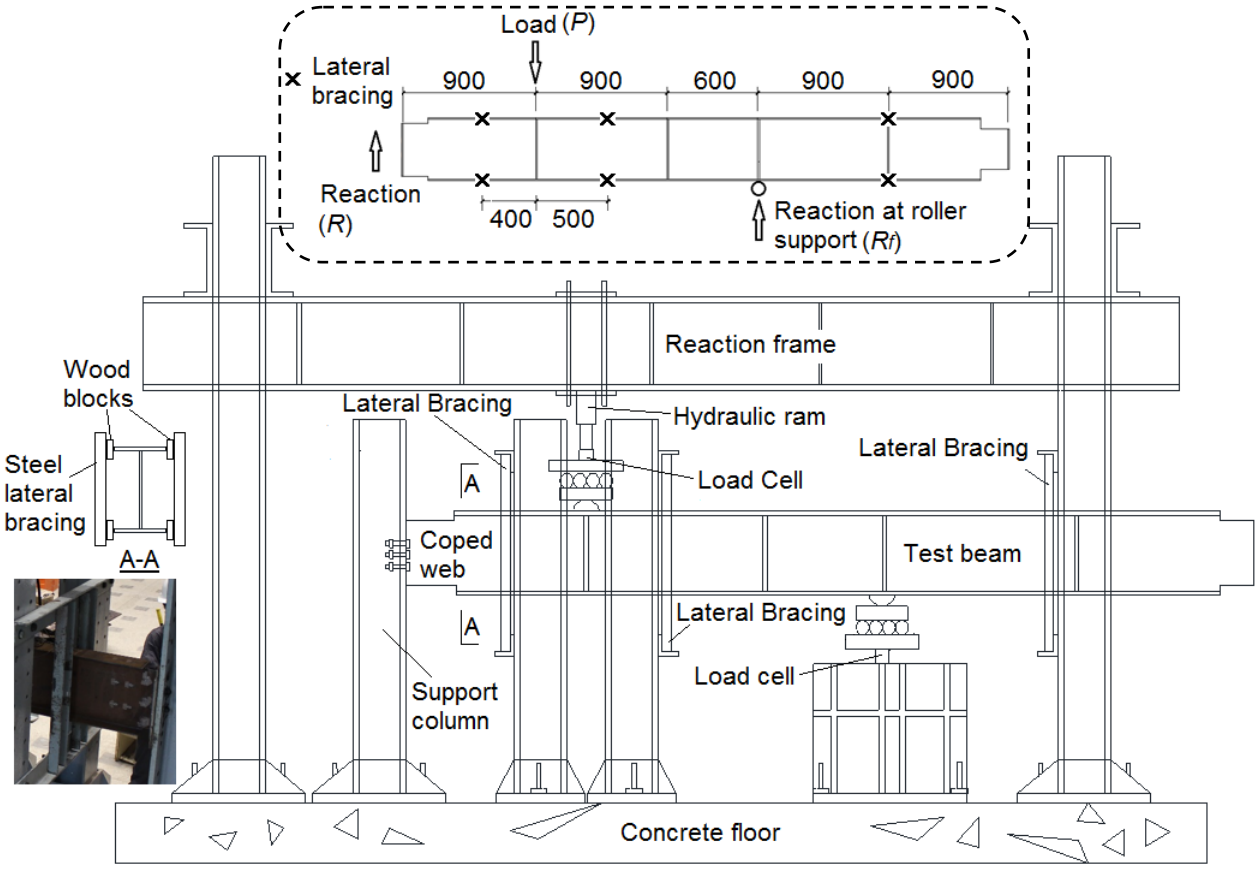

Fig. 3 Schematic illustrations and photos of test setup

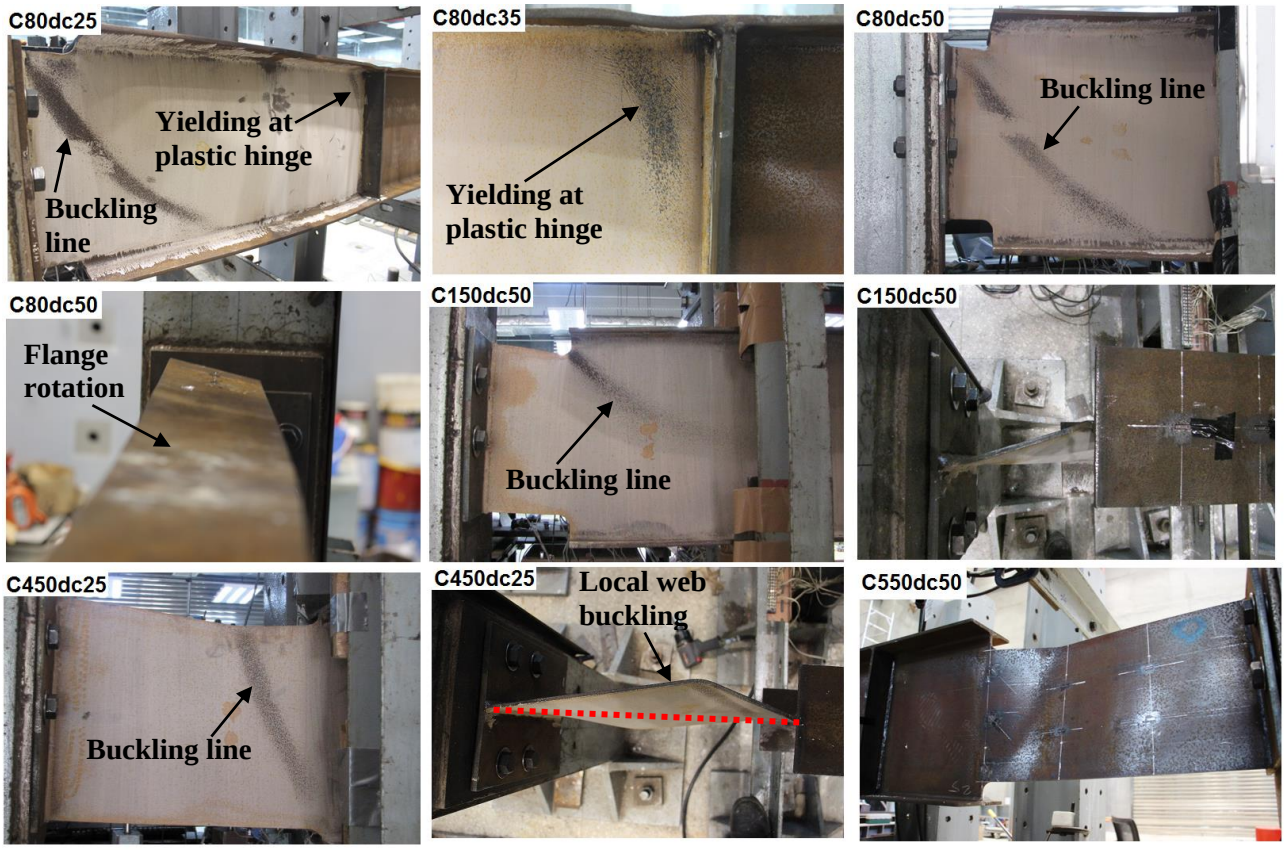

Fig. 4 Typical failure modes of specimens

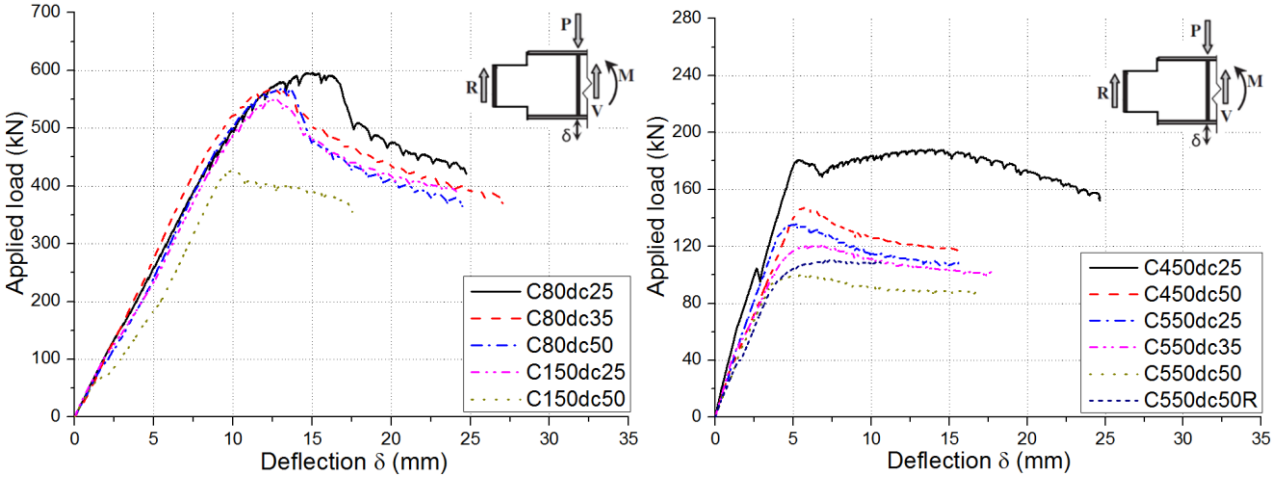

(a)

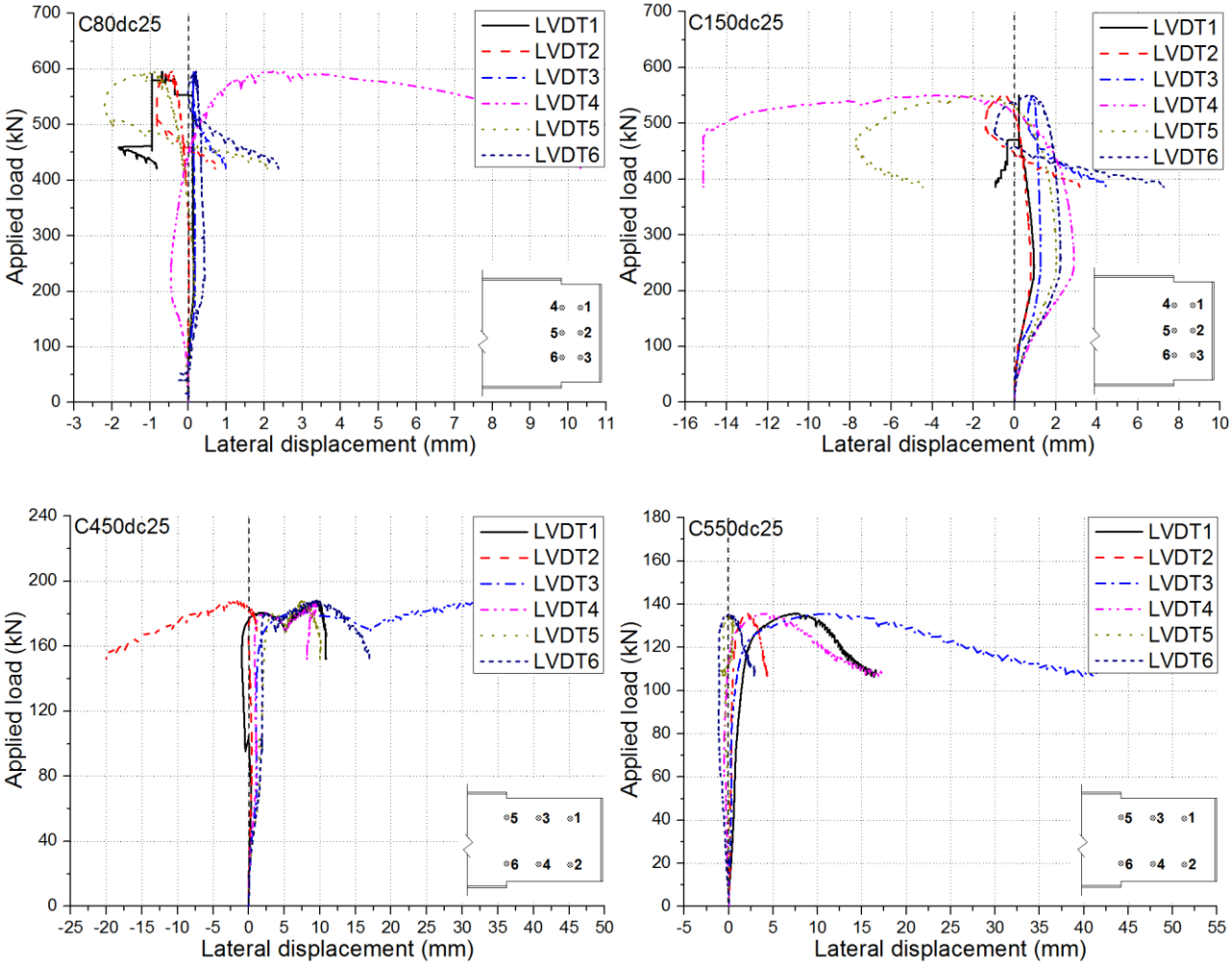

(b)

Fig. 5 Test results: a) load-vertical deflection response, b) load-horizontal deflection response

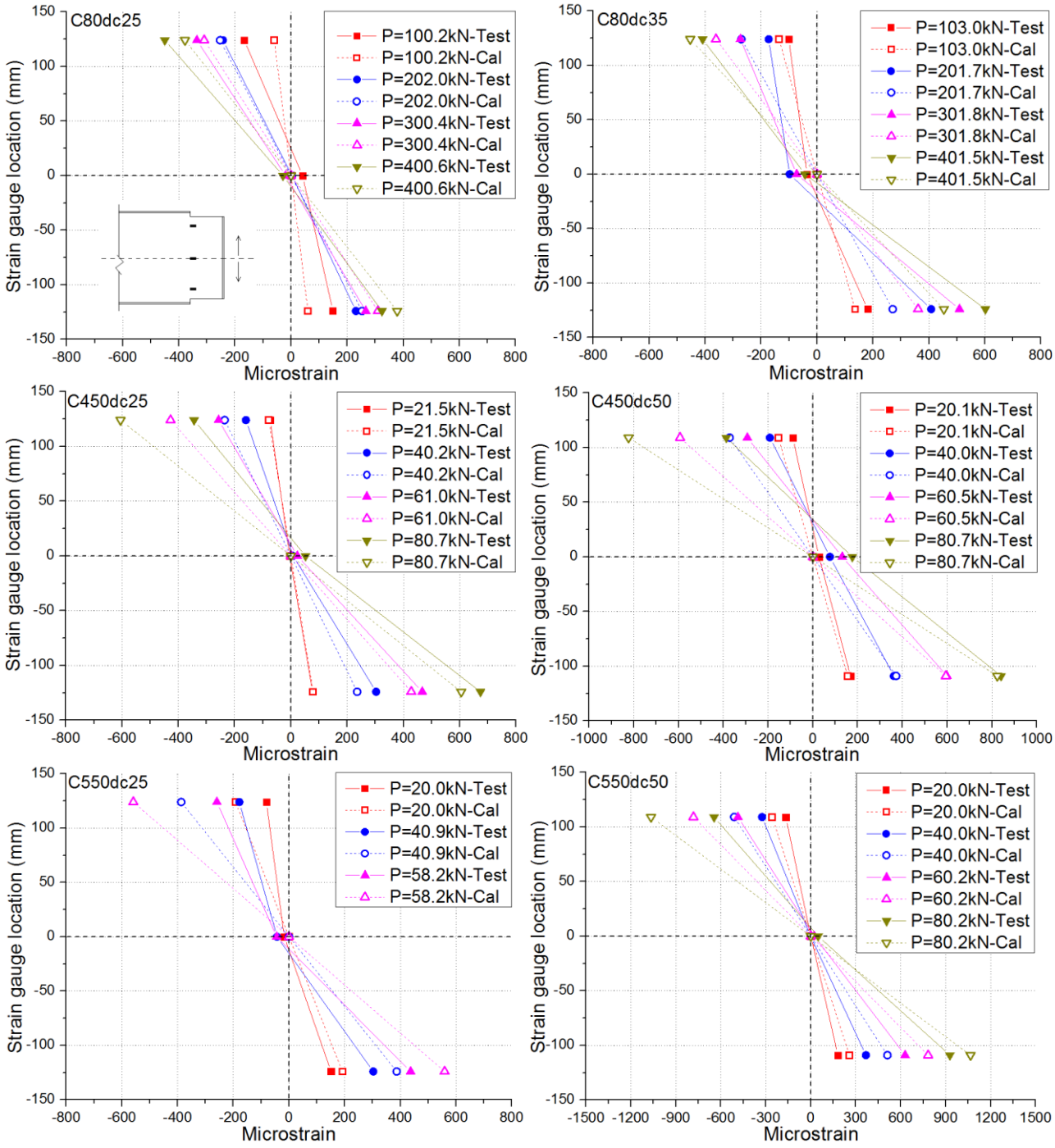

(a)

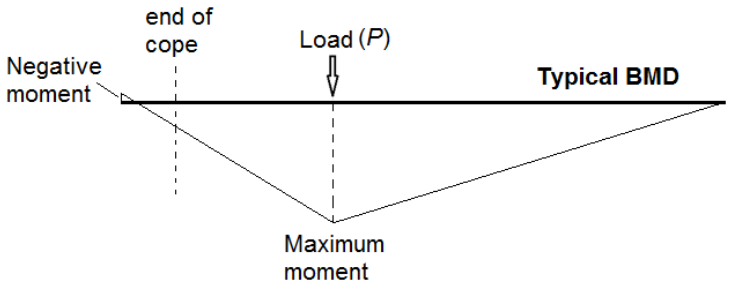

(b)

Fig. 6 Test results of strains: a) typical strain distributions, b) bending moment diagram for strain calculations

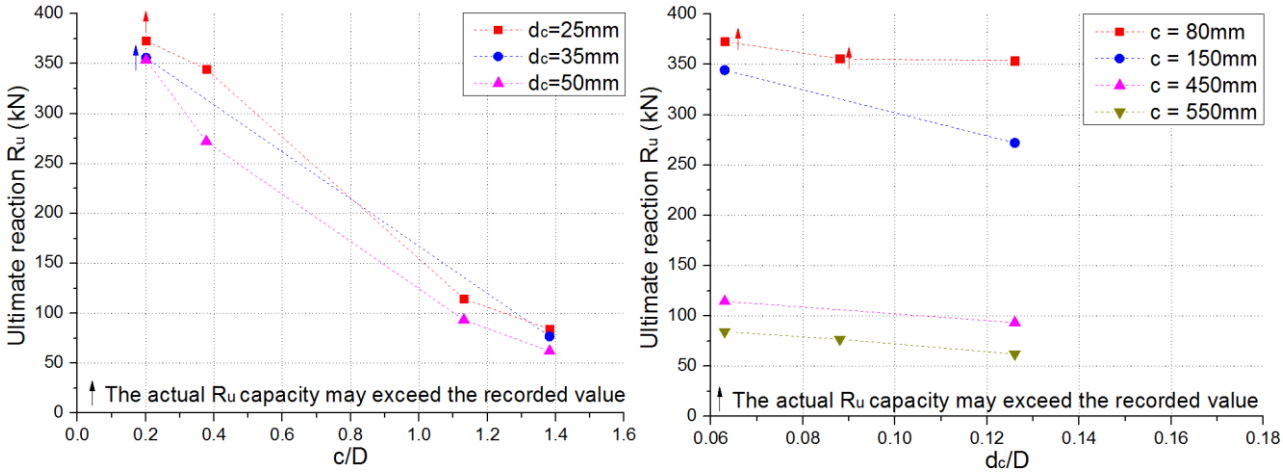

Fig. 7 Influences of coping details on ultimate reactions

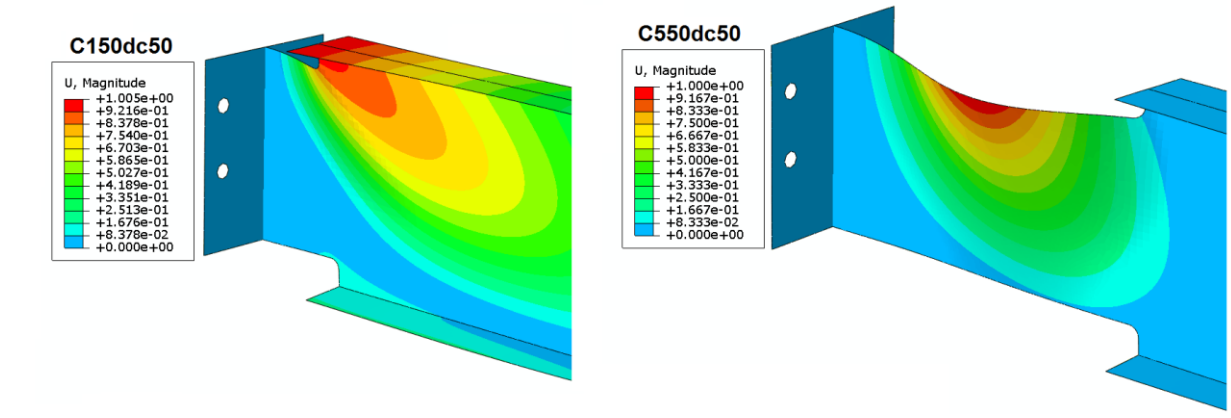

(a)

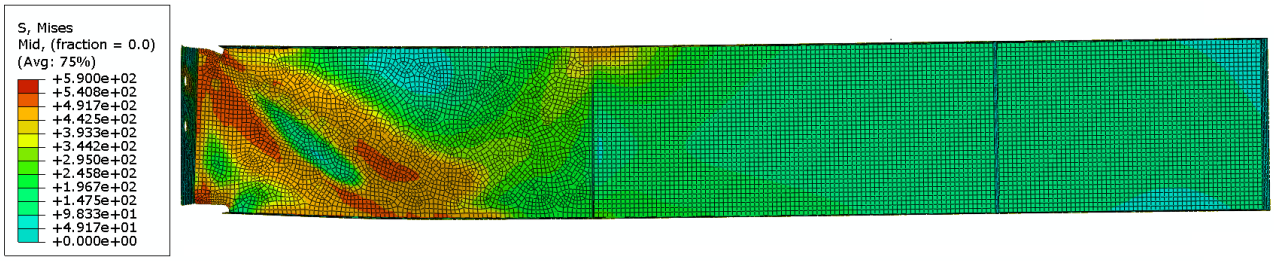

(b)

Fig. 8 Finite element analysis results: a) fundamental mode by eigenvalue analysis, b) local web buckling failure of ‘modified’ model C80dc25

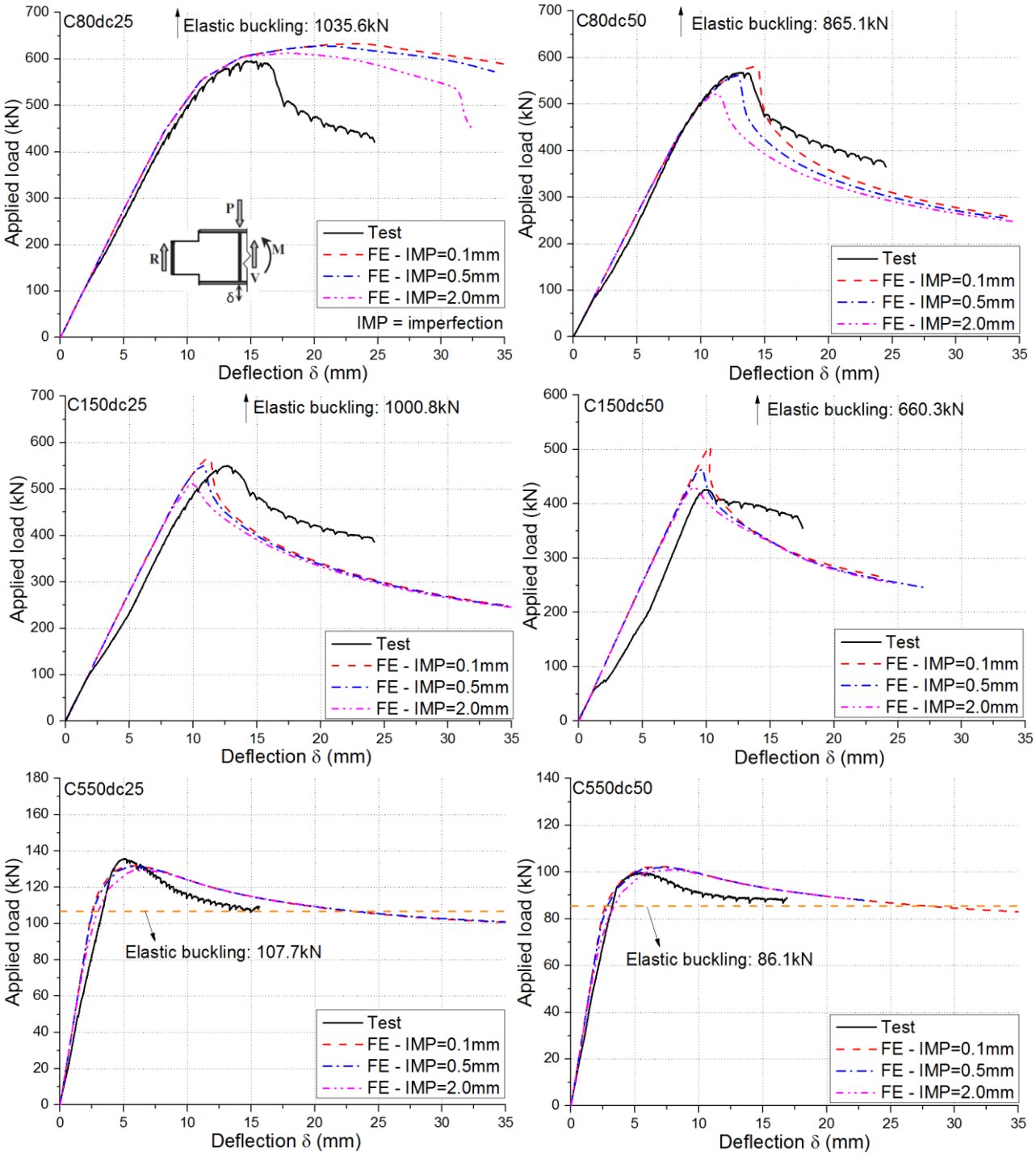

Fig. 9 Comparisons of load-deflection responses between test results and FE predictions

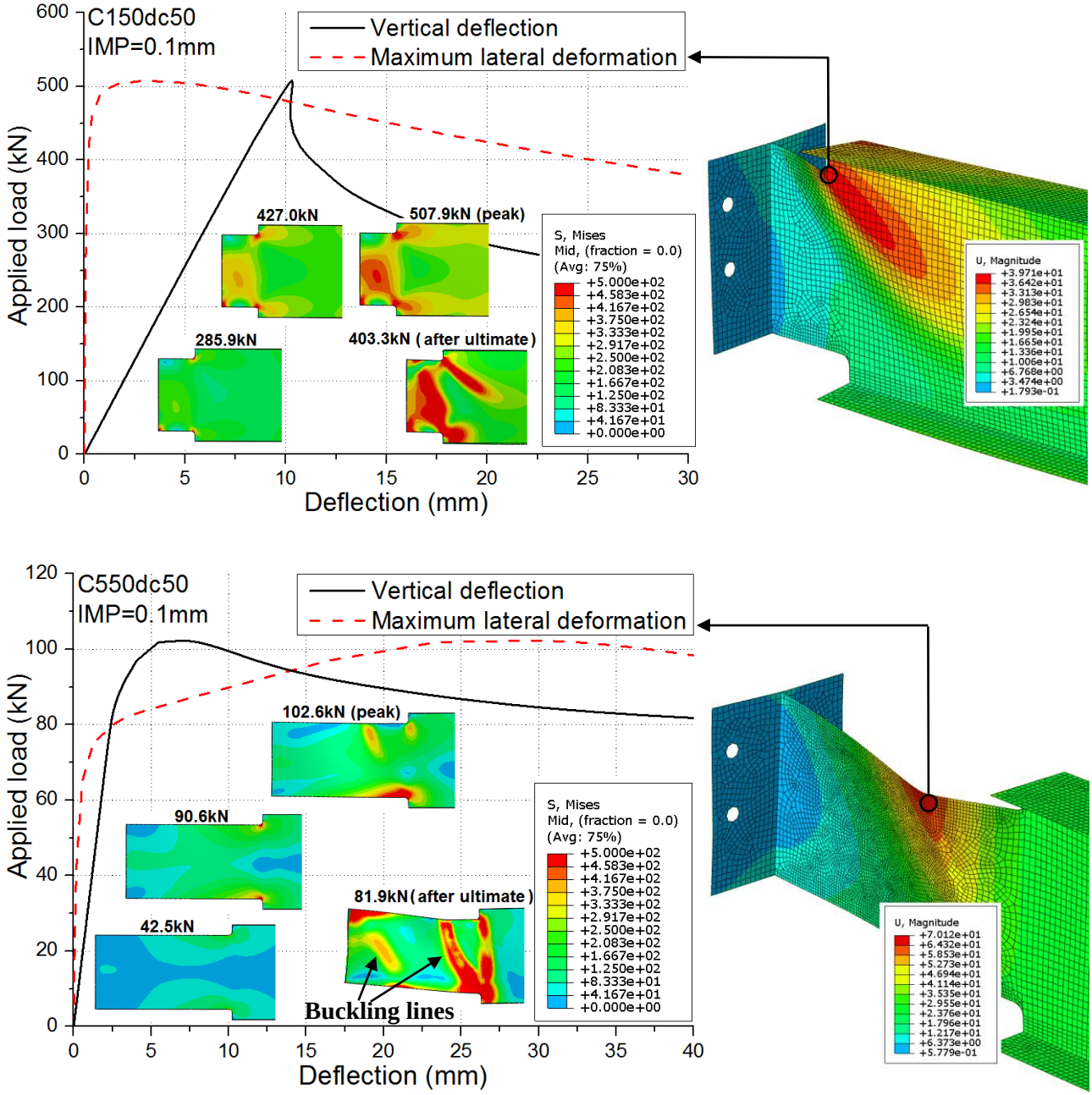

Fig. 10 Detailed load-deflection responses and stress conditions of typical specimens

Table 1 Key dimensions of specimens – measured values

Test specimens	Cope length c (mm)	Cope depth d_c (mm)	Web thickness t_w (mm)
C80dc25	80	24	6.19
C80dc35	80	34	6.19
C80dc50	80	49	6.15
C150dc25	150	24	6.15
C150dc50	148	49	6.14
C450dc25	450	24	6.12
C450dc50	450	49	6.12
C550dc25	550	24	6.23
C550dc35	550	34	6.23
C550dc50	550	49	6.19
C550dc50R	550	49	6.19

Table 2 Coupon test results for beam webs

Beam No.	Test specimens	Yield strength (MPa)	Ultimate strength (MPa)	Young's modulus (GPa)
Beam1	C80dc25 &C80dc35	456	587	193
Beam2	C80dc50 &C150dc25	486	621	201
Beam3	C150dc50	481	614	191
Beam4	C450dc25 &C450dc50	460	596	200
Beam5	C550dc25 &C550dc35	480	609	197
Beam6	C550dc50 &C550dc50R	475	608	202

Table 3 Summary of test results and design predictions

	Test specimens	c/D	d_c/D	Ultimate load P_u (kN)	Deflection at ultimate load Δ (mm)	Ultimate Reaction R_u (kN)	Ultimate end moment M_u (kN.m)	Negative moment length (mm)	R_y	R_{vy}	R_{cheng}	$\frac{R_u}{R_{design}}$
Current data	C80dc25	0.201	0.063	581.9#	15.6	372.8#	21.9	58.7	670.4	**567.3**	2452.1	-
	C80dc35	0.201	0.088	557.8#	12.7	355.8#	17.2	48.4	595.6	**534.7**	2167.4	-
	C80dc50	0.201	0.126	555.5^	13.2	353.7^	15.6	44.2	520.3	**514.1**	1736.5	0.69^
	C150dc25	0.377	0.063	541.9^	12.5	344.3^	13.5	39.1	**389.1**	600.4	702.3	0.88^
	C150dc50	0.377	0.126	424.4	10.0	272	16.2	59.6	**281.8**	507.8	505.4	0.97
	C450dc25	1.131	0.063	180.7	5.4	114.5	3.8	32.8	125.1	566.4	**79.4**	1.44
	C450dc50	1.131	0.126	146.7	5.7	93.4	4.1	44.0	91.6	484.4	**56.8**	1.64
	C550dc25	1.382	0.063	134.6	5.1	84.3	0.4	5.0	108.2	597.9	**54.8**	1.54
	C550dc35	1.382	0.088	120.2	6.1	76.8	4.0	52.3	96.1	563.7	**48.4**	1.59
	C550dc50	1.382	0.126	98.7	5.4	62.1	1.0	15.9	78.6	507.0	**39.6**	1.57
	C550dc50R	1.382	0.126	109.3	7.5	70.2	4.5	64.5	78.6	507.0	**39.6**	1.77
Fang et al. [21]	C300dc25	0.860	0.072	272.1	9.4	171.9	4.4	25.7	**102.7**	362.8	121.3	1.67
	C400dc25	1.146	0.072	170.2	10.5	107.8	3.4	31.7	77.6	364.1	**69.2**	1.56
	C500dc25	1.433	0.072	114.8	8.0	73.1	3.2	44.3	62.2	364.1	**44.4**	1.65
	C400dc50	1.146	0.143	125.3	8.7	79.3	2.4	29.9	53.9	303.7	**47.4**	1.67
	C400dc70	1.146	0.201	101.7	13.0	64.1	1.3	20.1	38.0	255.4	**32.9**	1.95
Aalberg [8]	A10	0.340	0.154	N/G	N/G	57.4	0	0	**69.0**	124.1	343.5	0.83
	A11	0.340	0.154	N/G	N/G	93.8	N/G	N/G	**69.0**	124.1	343.5	1.36
											Mean=	**1.424**
											CoV=	**0.262**

Note:
1) # at ultimate load, plastic hinge was formed at loading position.
2) ^ at ultimate load, yielding of beam occurred at loading position, but plastic hinge was not fully formed.
3) N/G: not directly given in the literature.
4) End-plate connections were used for all specimens except A11 where double angle cleats were used.
5) R_{design} = minimum value of R_y, R_{vy}, and R_{cheng}.